THE ROLE OF METAL SALT FILM FORMATION ON LOCALIZED CORROSION STABILIZATION

C.S. Brossia, D.S. Dunn and N. Sridhar
Center for Nuclear Waste Regulatory Analyses
Southwest Research Institute
6220 Culebra Road
San Antonio, TX 78228

ABSTRACT

The effect of salt film formation on the stabilization of corrosion in 1-dimensional simulated pits on Fe, Cr, Ni and Type 308 stainless steel was investigated in acidified chloride environments. Potentiostatic polarization and Raman spectroscopy revealed that both Fe and Ni form a metal-chloride salt film at the pit base that controls dissolution. Cr, on the other hand, exhibited a low dissolution rate compared to Fe and Ni and did not precipitate a chromium-chloride salt film even after polarization for long times. Dissolution of the salt film on Fe and Ni was observed to be an insufficient criterion for arrest of the high dissolution rates observed, highlighting the importance of the critical chloride concentration within the pit. The current-time behavior observed on polarization of a Type 308SS simulated pit showed evidence of precipitation of a salt film. Raman spectroscopy, indicated that the pit solution contained Cr-Cl complexes but no Fe-Cl nor Ni-Cl complexes were observed. Thermodynamic speciation modeling, coupled with the experimental work in this study, provided a better understanding of the role of the principal alloying elements of stainless steel on salt film formation and composition.

INTRODUCTION

The initiation and propagation of localized corrosion in Cl^- containing solutions are important considerations for evaluating the performance of many engineering structures. For components which are expected to retain their function for long periods, such as nuclear waste containers, prevention of pit growth is important because the pit propagation rates are high enough to penetrate thick walled containers in a relatively short period. Stable pit growth, or the continued propagation of pits without repassivation, occurs above the pitting potential, E_p (1). While pits may be initiated well below this potential, they repassivate spontaneously and thus do not propagate. Such pitting, called metastable pitting, is of fundamental importance to the understanding of localized corrosion dynamics, does not play a role in life prediction since these pits are shallow and do not perforate the engineered structure. The repassivation potential (E_{rp}) of stable pits occurs at potentials just below E_p

provided that E_{rp} is measured using deep pits with a slow backward potential scan rate and E_p is measured under long exposure conditions (2). Recently, initiation of crevice corrosion has been related to metastable pitting within crevices, thus unifying many electrochemical aspects of these two phenomena, at least for stainless steels in chloride solutions (3).

In performance assessment models, the experimentally measured repassivation potential is used as a simple threshold parameter for prediction of the occurrence of localized corrosion (4). However, it is important to provide a sound mechanistic basis for the repassivation potential. One mechanism that has been proposed for pit stabilization is the formation of a metal salt film at the bottom of pits (1). Prior to the formation of a salt film, the remnant of the passive film covering the metastable pits maintains the aggressive local chemistry of the pit electrolyte and prevents repassivation (5). In this local region, the chloride and metal cation concentrations may be sufficiently high to precipitate a metal chloride salt film. If the passive film cover is ruptured, mixing of the pit electrolyte with the more dilute external electrolyte results in repassivation of the metastable pits. However, if pits have sufficient rate of generation of aggressive electrolytes, then they may survive the rupture of passive film cover and continue to grow. While Laycock and Newman (1) argue that a salt film is necessary, others have shown that a critical level of chloride concentration, below the saturation concentration with repect to metal salt, is sufficient for pit propagation (6-8).

In prior investigations of salt film formation in pits of stainless steels, it has been assumed that saturation with respect to $FeCl_2$ dictates the condition for formation of the salt film (7, 9). Using X-ray fluorescence, Isaacs et al. (9) derived the composition of the salt film that developed in a 1-D simulated pit in Fe-18Cr-13Ni stainless steel to be enriched in Fe and depleted in Ni and Cr with respect to the alloy composition. The total metal cation concentration just above the salt film was calculated to be 5.0 M (3.4 M Fe, 1.1 M Cr, 0.5 Ni) exceeding the reported solubility limit of 4.4 M Fe^{2+} for $FeCl_2$ precipitation. Under the conditions studied, it was postulated that dissolution of the $FeCl_2$salt film controlled the rate of alloy dissolution and it was thought that the compositional make up of the salt film/saturated solution was due to differences in the effective diffusivity of the metal cations assuming stoichiometric dissolution within the pit. In these investigations, the speciation of pit solution and the effect of solution composition on solubility of metal chloride salt are generally not considered. Speciation may be important in understanding the critical solution composition needed for stable pit growth.

Despite the work on salt film formation in stainless steels, it is still unclear to what extent major alloying elements influence stable pit growth through formation of salt films, development of the critical chloride concentration in the pit solution, and control of dissolution kinetics of the bare metal in a concentrated chloride solution. Thus, the goals of this project are to (i) examine the nature and properties of salt films that form within simulated pits on the pure metal constituents of stainless steels as well as stainless steels and Ni-based alloys, and (ii) examine the composition of the solution above the salt film within the pit, with particular emphasis on metal-chloride complexes. Raman spectroscopy, potentiostatic polarization electrochemical impedance spectroscopy (EIS) and thermodynamic speciation modeling are used to investigate pitting kinetics and chemistry.

EXPERIMENTAL APPROACH

A four-port electrochemical cell (6) that enabled the introduction of a test specimen, Luggin probe with a Saturated Calomel electrode (SCE) as reference, a Pt or graphite counter electrode and a gas bubbler for N_2 purging was utilized. Further, one side of this cell was flat which allowed for easier focusing of the laser beam and permitted *in-situ* Raman spectroscopy of any films that precipitated on the electrode surface as well as analysis of the solution above the electrode. The test specimen was arranged such that it was close to the flat wall of the cell to minimize the path of the laser beam through the bulk solution, reducing Raman scattering from water.

All experiments were conducted with glass sheathed rods of either Fe (99.9985%), Cr (99.99%), or Type 308 stainless steel welding rod. The welding rod was chosen because of its low C content which minimized the potential for buildup of carbonaceous deposits at the pit base (6). The Fe rod was 2 mm in diameter with a glass sheath 10 mm in length protruding beyond the end of the rod, giving an aspect ratio of 0.2 (diameter/depth = 0.2). The Cr rod used was 4 mm in diameter with glass sheath 40 mm in length, giving an aspect ratio of 0.1. The experimental details concerning work examining the behavior of Ni is reported elsewhere (6). All tests were performed potentiostatically using an E.G.&G. Princeton Applied Research Model 273 potentiostat using front panel controls. All solutions were deaerated using N_2 gas and were made using reagent grade chemicals and high purity water (18 MΩ·cm).

Raman spectroscopy was conducted using a Kaiser Optical Holoprobe 532 dispersive system with a Coherent diode-pumped, solid-state, frequency-doubled Nd:YAG laser at 532 nm. The laser light is passed through optical fibers to the probe head which serves to focus the incident light and filter Rayleigh scattered light as well as Raman signal from the optical fiber. For examination for the presence of a salt film, the probe head was aligned at an oblique angle to enable the beam to be incident on the electrode surface. When used for examining the solution composition, the probe head was perpendicular to the electrode and was attached to a micrometer stage to enable concentration profiles to be determined.

In order to determine the speciation in aqueous solutions of metal chloride salts, Environmental Simulation Program (ESP), Version 6.0, developed by OLI Systems, was used. The equilibrium computations in ESP are based on a comprehensive thermodynamic model, which is applicable to aqueous systems. A detailed description of the model is given by Zemaitis et al. (10) and Rafal et al. (11). The model is based on the equation of state for standard-state properties developed by Helgeson and coworkers (12, 13). The Helgeson equation of state is coupled with techniques for estimating standard-state properties for species for which experimental data are missing (14-16). The activity coefficient model is based on the Bromley (17) theory for interactions between cations and anions and the Pitzer (14) model for ion-molecule and molecule-molecule interactions. The activity coefficient model is accompanied by techniques for estimating parameters in the absence of experimental data. These techniques are based on the work of Meissner (19) and the model substance concept. A Pitzer-type interaction model is also used to compute the density of the aqueous phase. All calculations using ESP V6.0 were performed assuming a temperature of 25°C and 1 atmospheric pressure.

EXPERIMENTAL RESULTS

Fe Simulated Pit

When the Fe simulated pit was polarized to 0.90 V_{SCE} in 0.5 M HCl + 2 M NaCl, the current density increased rapidly abruptly to over 100 mA/cm^2. After several minutes, the current density then began to decrease steadily at a rate proportional to $t^{0.55}$ to approximately 4 mA/cm^2. The current density then remained relatively stable, varying between 3-6 mA/cm^2. After over 500 min, a gel-like precipitate was observed at the base of the pit. With the Raman probe head positioned at a slightly oblique angle, the laser was then incident on the pit base which enabled *in-situ* determination of the composition of the precipitate. The Raman spectra of the precipitate as well as the spectra for $FeCl_2 \cdot 4H_2O$ are shown in Figure 1. Note that the intensity of the spectra for the precipitated film has been multiplied by a factor of 25 to facilitate viewing on the same scale as the $FeCl_2 \cdot 4H_2O$ solid salt. From this it is clear that the precipitated film is essentially $FeCl_2$ based on the peaks at 150, 175, 308 and 621 cm^{-1} (20). The peak at 490 cm^{-1} in the precipitated film spectra is likely associated with the hexaaquo complex $Fe(H_2O)_6^{2+}$ and glass, which has a broad peak at 480 cm^{-1}. The peaks found at 1635 and 1655 cm^{-1} are associated with H-O-H bond stretching in water (20). The sharpness of the precipitate peaks indicate that it is crystalline in nature.

To examine the role of the precipitated film in the propagation of corrosion, the potential was decreased in 0.45 V increments from 0.90 V_{SCE} after the film had stabilized. Figure 2 shows the potential decrease and the resulting current density response. Each decrease in potential resulted in an instantaneous decrease in the current density. Subsequently, the current density then began to rise, eventually attaining values higher than those measured prior to the potential change. These results were observed at potentials as low as -0.45 V_{SCE}, which is less than 0.20 V above the open circuit potential for the iron electrode in this environment. Furthermore, after the potential was decreased to 0 V_{SCE}, the precipitate that was present at the base of the pit dissolved and was no longer visible nor was Raman spectroscopy able to detect the presence of $FeCl_2$ at the pit base. The current density, however, still returned to values similar to those observed prior to the potential decrease. Even when the potential was decreased to -0.45 V_{SCE} the current density initially returned to near its original value before beginning steadily decrease prior to termination of the experiment.

Examination of standard $FeCl_2$ solutions revealed that Raman spectroscopy could be utilized to measure solution concentration, similar to the $NiCl_2$ solutions studied by Sridhar and Dunn (6). The standard $FeCl_2$ solutions were green in color as expected. However, no noticeable color changes were observed in the pit solution above the precipitated film and Raman spectroscopic analysis of pit solutions did not reveal the presence of Fe-Cl complexes in solution. When the bulk solution was changed from 0.5 M HCl + 2 M NaCl to 0.5 M HCl or to 0.5 M NaCl, the current-time behavior was indicative of precipitation of a salt film, however no color change was observed in the pit solution nor was Raman spectroscopy able to detect any dissolved Fe-Cl species.

Cr Simulated Pit

A similar electrode to that of Fe was constructed from Cr. On polarization of the Cr simulated pit electrode to 0.90 V_{SCE} in 0.5 M HCl, the current density initially decreased to a steady state value of 10 $\mu A/cm^2$ until approximately 150,000 s, during which time the solution in pit above the specimen began to take on a green hue (likely $CrCl_2^+$ or $CrCl^{2+}$). At 150,000 s, a sharp increase in the current density to nearly 0.35 mA/cm^2 was observed, after which the current density began a very gradual decrease to 70 $\mu A/cm^2$ after 667,000 s at which point the experiment was terminated. At no point was precipitation of a salt film observed, even though the color of the solution within the pit darkened with time. Further, no current transients that may indicate precipitation of a salt film were observed.

To identify and profile the concentration of the species in the pit solution as a function of depth, a series of Raman spectra as a function of $CrCl_3 \cdot 6H_2O$ concentration in 0.5 M HCl were taken. At this time, peak assignment to $CrCl_x^{(3-x)+}$ species has not been performed and hence the peak is referred to as Cr-Cl species. The peak area ratio of the peak associated with Cr-Cl species near 330 cm^{-1} and the water peak near 1655 cm^{-1} was fitted to the known concentration of standard solutions using a second order regression equation. Using the second order regression relationship between peak area ratio and concentration, the concentration profile of Cr-Cl species was determined (Figure 3). Even after long times (604,000 s), the maximum Cr-Cl concentration observed at the pit base was slightly less than 0.1 molal.

Type 308SS Simulated Pit

When a simulated 1-D pit was formed on Type 308SS and polarized to 0.90 V_{SCE} in 0.5 M HCl, current density (Figure 4) initially increased to over 100 mA/cm^2 then decreased to a short-lived steady state value of 35 mA/cm^2. The current density subsequently decreased to 15 mA/cm^2 then increased to 25 mA/cm^2 prior to reaching a steady state value of 9 mA/cm^2. Similar behavior associated with the precipitation of a salt film on Ni has been observed (6). The current density remained steady, even when the potential was decreased in 0.40 V increments from 0.90 to 0.10 V_{SCE}. When the potential was further decreased from 0.10 to -0.20 V_{SCE}, a current transient similar to that observed for Fe was seen in which the current instantaneously decreased and then asymptotically increased to its original value. When the potential was decreased to -0.40 V_{SCE}, the electrode repassivated.

The composition profile of the pit solution as a function of time was determined using Raman spectroscopy. Comparison of the spectra obtained from the pit solution to spectra from solutions of $CrCl_3 \cdot 6H_2O$, $FeCl_2 \cdot 4H_2O$ and $NiCl_2 \cdot 6H_2O$ as well as the solid salts revealed that the dominant species being observed using Raman spectroscopy were aqueous Cr-Cl complexes (Figure 5). Based on the approach outlined in the previous section, the concentration of Cr-Cl species in the pit solution was calculated and is shown as a function of potential in Figure 6. Each profile was obtained after the potential had been held for over 24 hr (86,400s). Because the dissolution rate was nominally constant even after the potential was systematically decreased from 0.90 to 0.10 V_{SCE}, the concentration of Cr-Cl species either was nearly constant with potential or increased slightly, especially near the pit base. After the potential was decreased to -0.40 V_{SCE}, the concentration of Cr-Cl species in the pit solution decreased significantly and was nearly constant for all depths in the pit.

Equilibrium Speciation Calculations

Few studies have considered the speciation of solution inside pits. Verbrugge et al. (21) suggested that the dominant species in a pit on pure Ni were aqueous $NiCl_2$ and $NiCl^+$. Sridhar and Dunn (6) suggested that the dominant species is more likely to be the hexaaquo complex $Ni(H_2O)_6^{2+}$ and that this is more consistent with literature data than the presence of aqueous $NiCl_2$. The speciation is important in the pit because neutral species such as $(NiCl_2)_{aq}$ do not migrate under potential gradients whereas charged cations such as Ni^{2+} and $NiCl^+$ may be transported away from the bottom of a pit rapidly under a potential gradient. Similarly, it has been hypothesized that negatively charged molybdate may inhibit pit growth by minimizing chloride migration towards the pit bottom. Additionally, the solubility of metal chloride salt in pit electrolyte is important in some models of pit initiation (1,3), but the effect of solution composition on solubility has not been considered in the literature.

The equilibrium speciation in pure Fe, Cr, and Ni, as calculated by the thermodynamic code ESP, is shown in Figure 7. In the case of Fe and Ni, the dominant species is the hexaaquo cation, $M(H_2O)_6^{2+}$ which is shown in Figure 7 as M^{2+} for simplicity. However, unlike the case of Ni, where only the chloride complex $NiCl^+$ is stable, both the charged $FeCl^+$ and the neutral $(FeCl_2)_{aq}$ are stable for the case of Fe. The solubility of $FeCl_2$ in a 0.5M HCl is about 5 molal whereas that of $NiCl_2$ is 4.8 molal. Beyond these concentrations, precipitation of hydrated salts occur as shown in Figure 7. Although, the activity of the solid phase remains equal to 1, the amount precipitated increases as would be expected from mass balance considerations. The amount of precipitated salt is plotted on the concentration scale for simplicity. $CrCl_3$ has a much higher solubility as predicted by the code, although in reality solutions with greater than 10 molal $CrCl_3$ could not be prepared. In the case of $CrCl_3$, the dominant species at high concentrations is $CrCl^{2+}$, whereas below 1 molal both the hexaaquo complex, $Cr(H_2O)_6^{3+}$, and $CrCl^{2+}$ are present in approximately equal concentrations.

The speciation in mixtures of $FeCl_2$, $CrCl_3$, and $NiCl_2$ is important for the localized corrosion of stainless steel. Assuming that type 308 SS dissolves congruently, the speciation of solutions in which the ratio of Ni:Fe:Cr was kept at 1:6.6:2.01 was examined (Figure 8). For comparison, the speciation of pure metals is also plotted in these graphs. The speciation of each component is shown as a function of total metal dissolved. It can be seen that for a given total metal dissolved, the predominant ionic species are Fe^{2+} and $CrCl^{2+}$. It can also be seen that although precipitation of $NiCl_2.6H_2O$ from the alloy occurs at a greater concentration of total metal dissolved than in the case of pure metal, since the total concentration of Ni(II) in the mixture is only about 0.1 times the total concentration, the solubility of Ni(II) is actually lower in terms of equivalent Ni dissolved in the mixture than in pure $NiCl_2$ solution. This suggests that if sufficient alloy dissolves, $NiCl_2$ may coprecipitate with $FeCl_2$.

DISCUSSION

Previous work (6) on examining simulated pits on Ni revealed that a relatively thick $NiCl_2$ salt film precipitated after potentiostatic hold at 1.50 V_{SCE} for long periods of time. EIS and Raman spectroscopy data revealed that the salt film disappeared when the potential decreased below 0 V_{SCE}, but stable pit growth was still observed at potentials as low as

-200 mV_{SCE}. This result thus shows that dissolution of the salt film is not sufficient for repassivation of pit growth to occur in Ni. Thus, this highlights the importance of the critical chloride concentration in the pit site as playing a key role in repassivation of Ni. Further analysis revealed that the critical $NiCl_2$ concentration required for repassivation was 17% of saturation for $NiCl_2$.

In the present work, Fe was similarly observed to form a salt film at the base of the simulated pit which aided in stabilizing rapid dissolution. *In-situ* Raman spectroscopy revealed that the salt film was principally composed of $FeCl_2$, as has been determined by others examining localized corrosion of Fe using indirect determinations such as visual observation (22) and limiting current calculations (23). Other peaks at 709 and 1413 cm^{-1} may indicate the presence of γ-Fe_2O_3, which exhibits strong Raman peaks at 717 and 1412 cm^{-1} (24). Due to the relative intensity of these peaks, however, it seems likely that the principal composition of the precipitate is $FeCl_2$. Similar to Ni, Fe was also observed to continue pit propagation even after Raman spectroscopy revealed that $FeCl_2$ was no longer present at the pit base at 0 V_{SCE}. It could be argued that the resolution of Raman spectroscopy was insufficient to detect a very thin salt precipitate that may still have been present. A limited study examining salt film properties as a function of potential using EIS revealed that a significant change occurs between 0 and -0.15 V_{SCE}, which is in line with the behavior observed during potentiostatic polarization. The works by others also clearly demonstrates that potentials significantly less than 0 V_{SCE} are outside the stable potential regime for $FeCl_2$ precipitation (22, 23, 25), as these works have focused attention at considerably higher potentials. The dissolution rate at 0 V_{SCE}, however, was still comparable to that observed when the film was still intact. When the potential was further decreased to -0.45 V_{SCE}, the current density rebounded to its original value after an initial decrease and then after a short time began a steady decrease. This again points to the importance of a critical solution chemistry within the occluded region as a controlling factor for sustainment of high dissolution rates even in the absence of a salt film.

Raman spectroscopy of the pit solutions did not reveal the presence of Fe-Cl complexes in solution nor was a color change in the pit solution observed visually as would be expected if significant concentrations of Fe-Cl aqueous complexes were present. Thermodynamic speciation modeling (Figure 7) revealed that up to precipitation of $FeCl_2 \cdot 4H_2O$, the hexaaquo complex $Fe(H_2O)_6^{2+}$ is the dominant dissolved iron species as compared to $FeCl^+$. The maximum predicted concentration for $FeCl^+$ at $FeCl_2 \cdot 4H_2O$ precipitation is approximately 0.1 molal. The actual concentration in the pit solution may be lower as the thermodynamic model assumes that the Cl^- concentration in the solution is always twice the concentration of dissolved Fe present, which may not be the case in the pit solution in which Cl^- must migrate into the pit. Thus, the lack of significant color change in the pit solution and the reason why Raman spectroscopy did not detect $FeCl^+$ in the pit solution is because the dissolved iron was present predominantly as $Fe(H_2O)_6^{2+}$.

The simulated pit on Cr behaved significantly different than that for Ni and Fe, as might be expected. A very low dissolution rate was observed, never exceeding 1 mA/cm^2, even at 0.90 V_{SCE} in 0.5 M HCl. Furthermore, no current transients indicative of the formation of a salt precipitate were observed and Raman spectroscopy of the pit base did not reveal the presence of a hydrated Cr-Cl salt, even after 185 hrs of polarization. To help identify the nature of the Cr-Cl species present in the pit solution, thermodynamic speciation

calculations were performed using OLI software (Figure 8), indicating that the dominant Cr-Cl species present was $CrCl^{2+}$. Comparison of electrochemical kinetics and the concentration of $CrCl^{2+}$, though, shows that considerably more Cr was produced than can be accounted for by the $CrCl^{2+}$ present. At the concentrations of $CrCl^{2+}$ measured in the pit solutions, thermodynamic modeling predicts that the dominant dissolved Cr species would be the hexaaquo Cr complex $Cr(H_2O)_6^{3+}$. Thus, it seems likely that in addition to $CrCl^{2+}$, considerable quantities of $Cr(H_2O)_6^{3+}$ were also present.

The behavior observed for the simulated pit on Type 308SS exhibited current-time behavior that may indicate precipitation of a salt film at the pit base (6). Raman spectroscopic analysis of the pit base was unable to delineate the composition of the salt film due to the buildup of a black deposit on the surface, similar to what has been observed on commercially pure Ni (6). Based on the works of Steinsmo and Isaacs (7) and Isaacs et al. (9), the salt film would be composed principally of $FeCl_2$, with approximately 6% Ni and 1% Cr also present. Isaacs et al. (9), if present though, reported that the pit solution composition just above the salt film was nearly stoichiometric with respect to the alloy composition, being only slightly enriched in Cr^{3+} and slightly depleted in Ni^{2+}. It was claimed that assuming stoichiometric dissolution of the alloy, that this disparity in the compositions of the salt film and the pit solution were due to the relative diffusivities of the metal cations through the salt film, in the order of $D_{Cr} > D_{Ni} > D_{Fe}$.

Based on the thermodynamic speciation work in the present study, an alternate explanation for the possible composition and nature of the salt film and the solution above the salt film can be proposed. Thermodynamic modeling has shown that the dominant dissolved species in the pit are $Fe(H_2O)_6^{2+}$ and $CrCl^{2+}$, with smaller concentrations of other species also present (Figure 8). Further, experimental work with the simulated Cr pit and speciation modeling demonstrated precipitation of $CrCl_3$ did not occur, and likely would not occur until very high concentrations of dissolved Cr were reached. In fact, the only dissolved metal-chloride species detected in the pit solution for Type 308 was $CrCl^{2+}$, adding further evidence for this. Thus, with respect to the composition of a salt film that could form on stainless steel, one would expect it to be $FeCl_2$ with little or no Cr, as $CrCl_3$ precipitation is unlikely; small concentrations of Ni may also be present in the salt film as the solubility for $NiCl_2 \cdot 6H_2O$ was significantly diminished in the presence of other metal chlorides.

Repassivation of Type 308 occurred only when the potential was decreased to $-0.40\ V_{SCE}$. It is unclear if salt film dissolution occurred prior to this at higher potentials, as no experimental observation to this effect was made. In terms of repassivation of stable pits in Type 308SS, the following observations were made in the present study that may shed light on this. It was observed that the $CrCl^{2+}$ concentration and the dissolution rate were essentially unaffected by potential until $-0.40\ V_{SCE}$, that if a salt film was present it would likely be principally composed of $FeCl_2 \cdot 4H_2O$, with coprecipitated $NiCl_2 \cdot 6H_2O$ possibly also present. Because repassivation of both Fe and Ni was not predicated on dissolution of their respective salt films, but rather on the pit solution chemistry, it seems likely then based on these results and the works by Steinsmo and Isaacs (7) and Gaudet et al. (8), that repassivation of Type 308SS similarly does not depend on dissolution of the salt film, but rather on the chloride concentration in the pit solution.

SUMMARY

1. Fe and Ni both precipitate a metal-chloride salt film at the pit base which controls dissolution. When the potential was decreased such that the film became unstable and dissolved, high dissolution rates were still observed highlighting the importance of the solution chemistry within the occluded region.

2. Cr was observed to have a low dissolution rate in comparison to Fe and Ni and did not precipitate a Cr-Cl salt film even after polarization for 185 hr.

3. Polarization of a Type 308SS simulated pit resulted in the formation of a salt film, most likely through coprecipitation of $NiCl_2 \cdot 6H_2O$ and $FeCl_2 \cdot 4H_2O$. The only dissolved metal-chloride species observed in the pit solution was $CrCl^{2+}$. Evidence seems to suggest that repassivation of Type 308 under the conditions studied is more dependent on the pit solution chemistry than the dissolution of the salt film.

4. Thermodynamic speciation modeling has been found to be useful tool and has shown that the solubility limit for both Fe and Ni chloride salts decrease significantly in the present of other metal chlorides. It has also helped reveal the speciation of the pit solution and confirmed what was observed experimentally.

ACKNOWLEDGMENTS

This work was funded by the U.S. Nuclear Regulatory Commission (NRC), Office of Nuclear Materials Safety and Safeguards, Division of Waste Management under contract No. NRC-02-97-009. This work is an independent product of the Center for Nuclear Waste Regulatory Analyses and does not necessarily reflect the views or the regulatory position of the NRC. The technical assistance of M. Bogart and reviews performed by Drs. G.A. Cragnolino and B. Sagar (Center for Nuclear Waste Regulatory Analyses) are appreciated. Helpful technical discussions with Dr. H.S. Isaacs (Brookhaven National Laboratory) are also appreciated.

REFERENCES

1. N.J. Laycock and R.C. Newman, Corrosion Science, 39, 1771 (1997).
2. D.S. Dunn, N. Sridhar, and G.A. Cragnolino, Corrosion, 52, 115 (1996).
3. N.J. Laycock, J. Stewart, and R.C. Newman, Corrosion Science, 39, 1791 (1997).
4. S. Mohanty, G.A. Cragnolino, T. Ahn, D.S. Dunn, P.C. Lichtner, R.D. Manteufel, and N. Sridhar, Engineered Barrier System Performance Assessment Code: EBSPAC Version 1.1 - Technical Description and User's Manual, CNWRA 97-006, San Antonio, TX: Center for Nuclear Waste Regulatory Analyses (1997).
5. G.S. Frankel, L. Stockert, F. Hunkeler and H. Boehni, Corrosion, 43, 429 (1987).
6. N. Sridhar and D.S. Dunn, J. Electrochem. Soc., 144, 4243 (1997).
7. U. Steinsmo and H.S. Isaacs, J. Electrochem. Soc., 140, 643 (1993).
8. G.T. Gaudet, W.T. Mo, T.A. Hatton, J.W. Tester, J. Tilly, H.S. Isaacs and R.C. Newman, AIChE J., 32, 949 (1986).
9. H.S. Isaacs, J.-H. Cho, M.L. Rivers, and S.R. Sutton, J. Electrochem. Soc., 142, 1111 (1995).

10. J.F. Zemaitis, Jr., D.M. Clark, M. Rafal, and N.C. Scrivner, 1986, Handbook of Aqueous Electrolyte Thermodynamics, AIChE, New York, NY, (1986).
11. M. Rafal, J.W. Berthold, N.C. Scrivner, and S.L. Grise, in Models for Thermodynamic and Phase Equilibria Calculations, 601-670, S.I. Sandler Editor, M. Dekker, New York, NY (1995).
12. H.C. Helgeson, D.H. Kirkham and G.C. Flowers, Am. J. Sci., 281,1249 (1981).
13. J.C. Tanger and H.C. Helgeson, Am. J. Sci., 288, 19 (1988).
14. E.L. Shock and H.C. Helgeson, Geochim. Cosmochim. Acta, 52, 2009 (1988).
15. E.L. Shock and H.C. Helgeson, Geochim. Cosmochim. Acta, 54, 915 (1990).
16. D.A. Sverjensky in Reviews in Mineralogy, I.S.E. Carmichael and H.P.Eugster Editors, Mineralogical Society of America, vol. 17, Washington, D.C. (1987).
17. L.A. Bromley, AIChE J., 19, 313 (1973).
18. K.S. Pitzer, J. Phys. Chem., 77, 268 (1973).
19. H.P. Meissner, AIChE Symposium Series, 173, 74 (1978).
20. S. Bruni, F. Cariati, P. Fermo, G. Spinolo and M. Martini, J. Phys. Chem. Solids, 59, 845 (1998).
21. M.W. Verbrugge, D.R. Baker, and J. Newman, J. Electrochem. Soc., 140, 2530 (1993).
22. T.R. Beck, J. Electrochem. Soc., 129, 2412 (1982).
23. H.C. Kuo and D. Landolt, Corrosion Science, 16, 915 (1976).
24. D.L.A. de Faria, S. Venancia Silva and M.T. de Oliveira, J. Raman Spectroscopy, 28, 873 (1997).
25. R.D. Grimm, A.C. West and D. Landolt, J. Electrochem. Soc., 139, 1622 (1992).

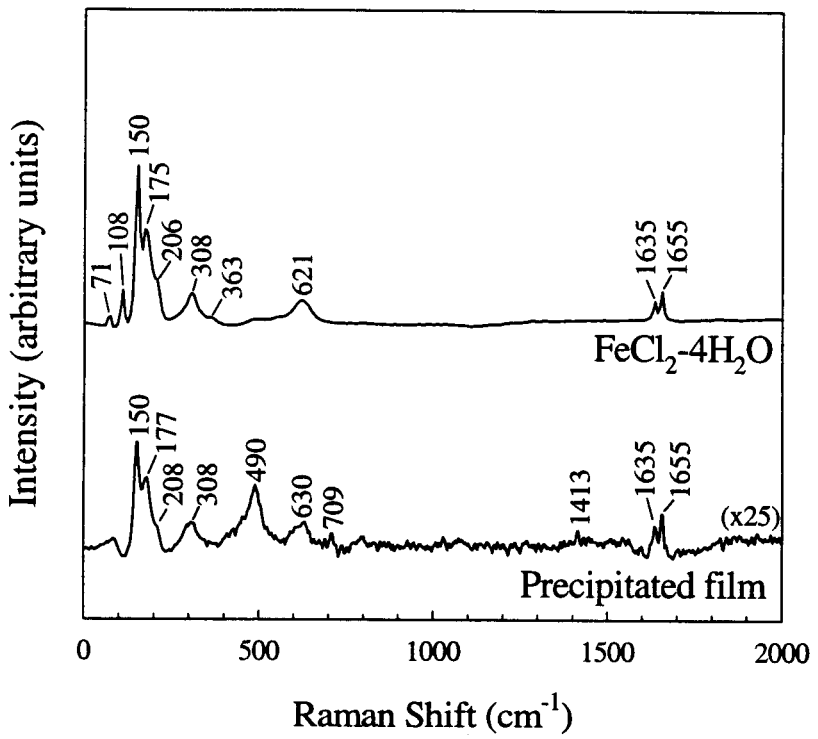

Figure 1: Raman spectra of $FeCl_2 \cdot 4H_2O$ and precipitated film formed in 1-D pit on Fe.

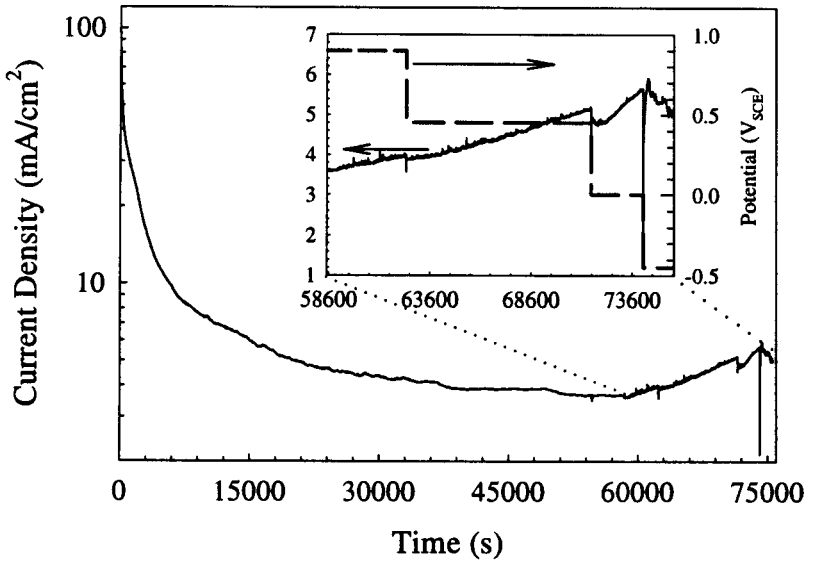

Figure 2: Current-time behavior for 1-D simulated pit on Fe initially polarized to 0.9 V_{SCE} in an acidified chloride solution. The inset shows the effects of systematically decreasing the potential on the measured current density.

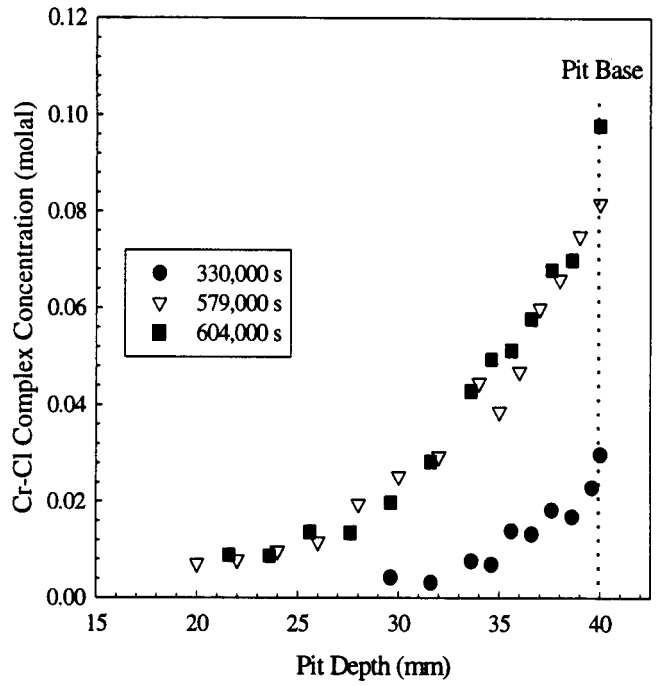

Figure 3: Concentration profiles for dissolved Cr-Cl complexes as a function of time for a 1-D simulated pit on Cr at 0.9 V_{SCE} in 0.5 M HCl.

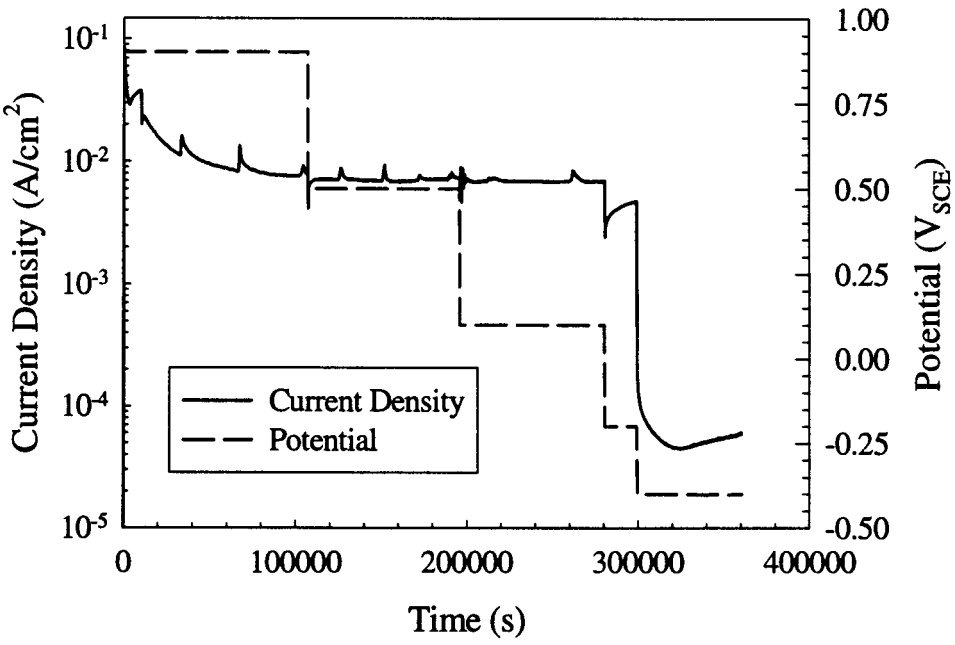

Figure 4: Current-time behavior observed for 1-D simulated pit on Type 308SS in 0.5 M HCl as a function of applied potential.

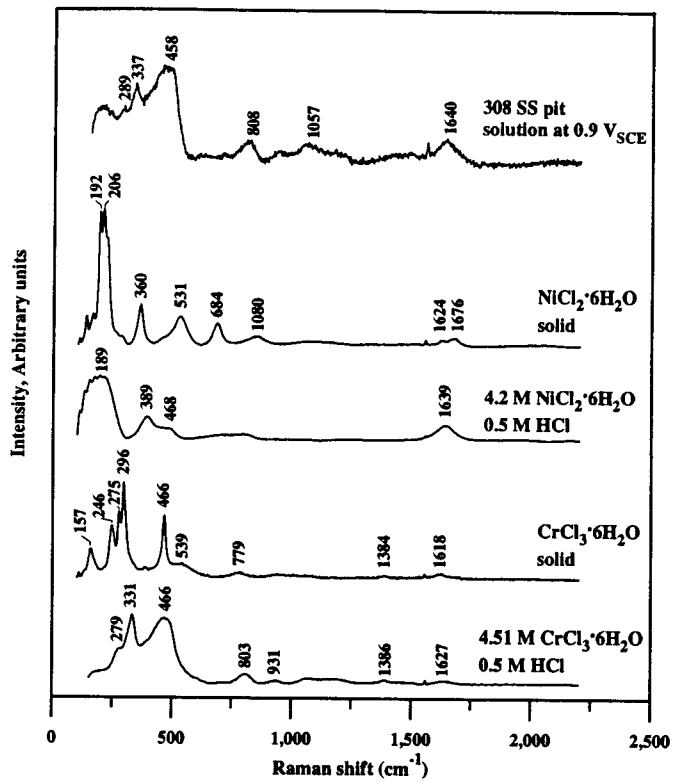

Figure 5: Raman spectra for $NiCl_2 \cdot 6H_2O$ and $CrCl_3 \cdot 6H_2O$ solid salts and solutions along with the Raman spectra for the Type 308SS pit solution.

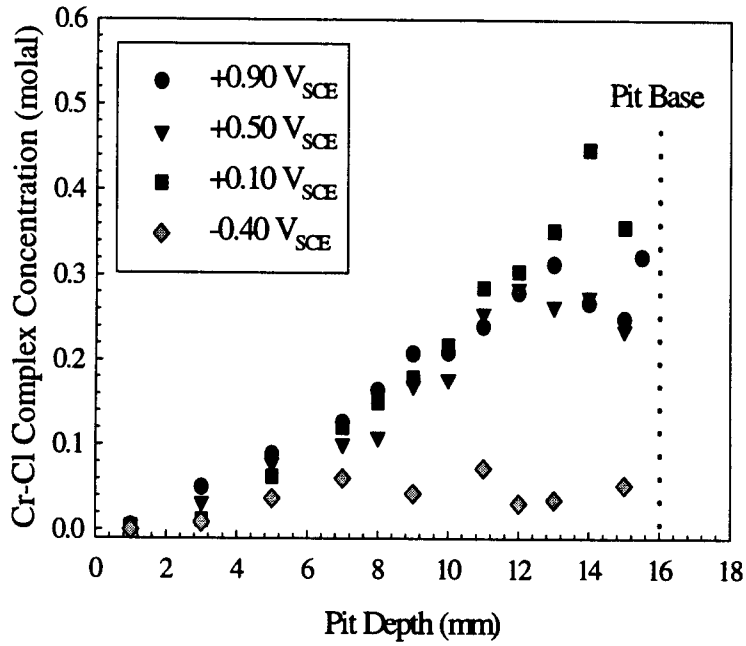

Figure 6: Concentration profile for aqueous Cr-Cl complexes in 0.5 M HCl as a function of applied potential for Type 308SS simulated pit.

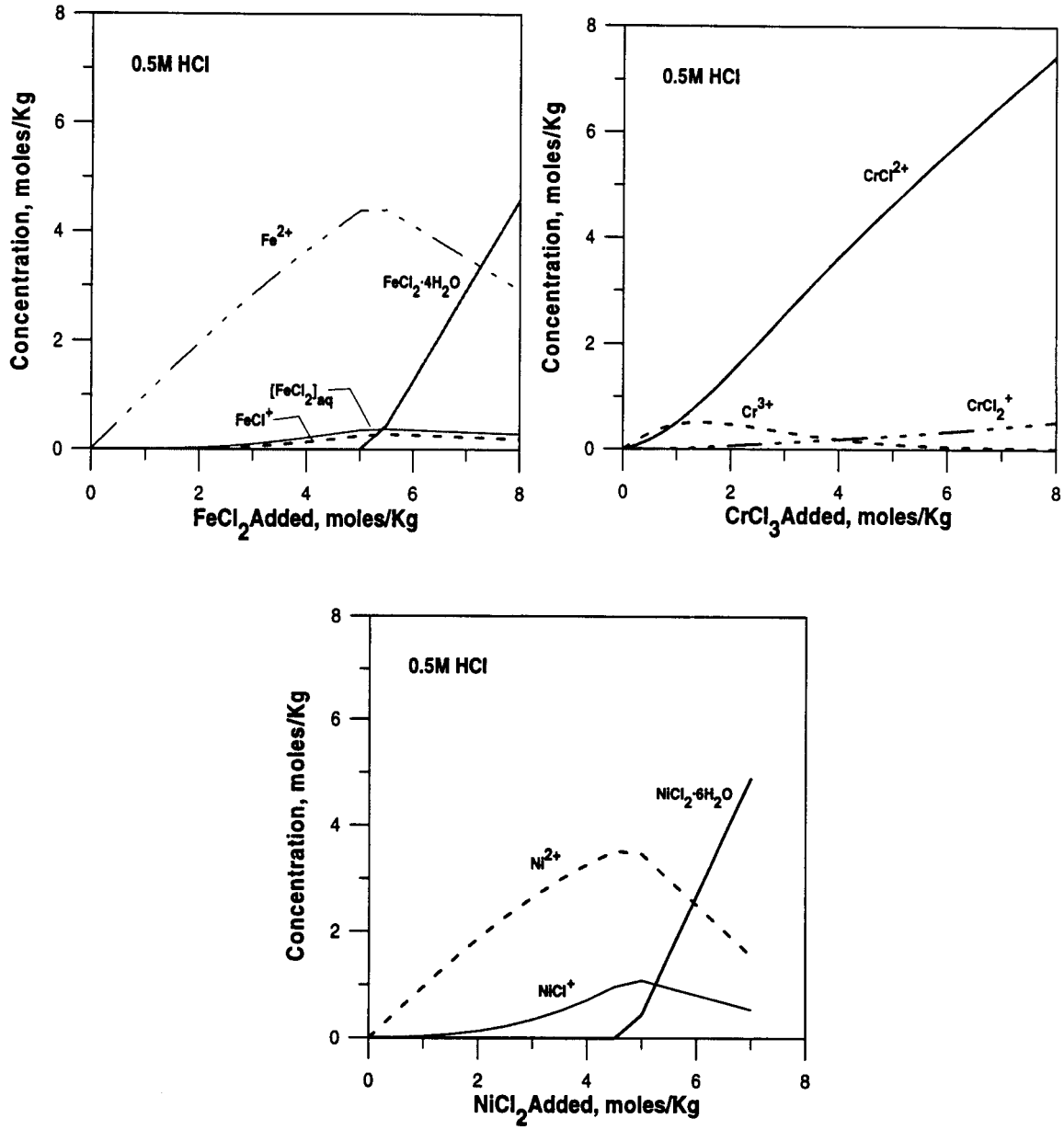

Figure 7: Predicted speciation of Fe, Cr, and Ni in pure chloride solutions.

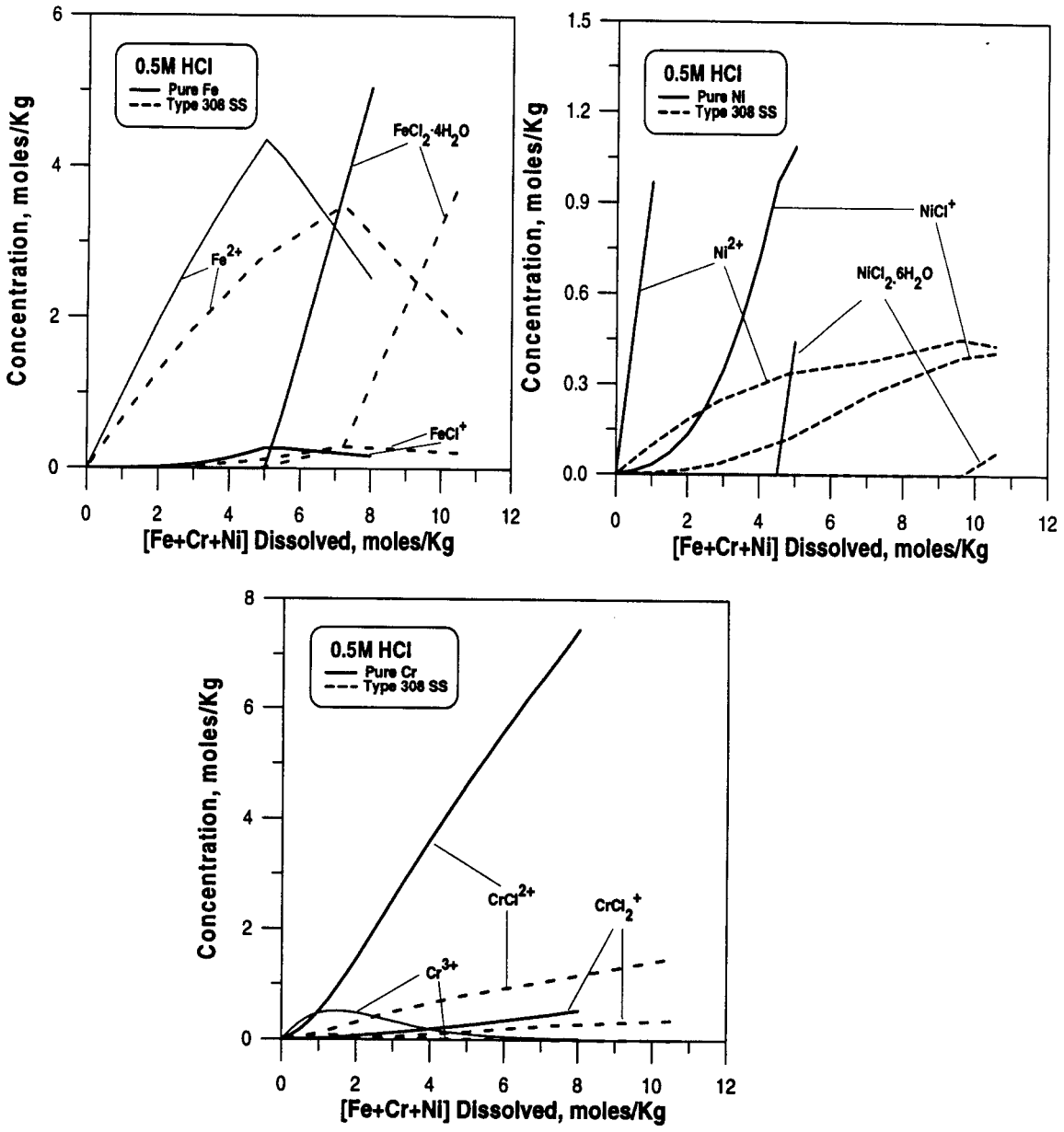

Figure 8: Speciation in mixtures of $NiCl_2$, $FeCl_2$, and $CrCl_3$ solution assumed to be formed from congruent dissolution of type 308 stainless steel (Fe:Cr:Ni = 6.6:2.01:1).